Correlation between chromium physicochemical properties in silicate melts and the corrosion behavior of chromia-forming alloy

Eric Schmucker, Carine Petitjean, Pierre-Jean Panteix, Laure Martinelli, Sabah Ben Lagha, Michel Vilasi

Correlation between chromium physicochemical properties in silicate melts and the corrosion behavior of chromia-forming alloy

Eric Schmucker[1,3*], Carine Petitjean[1], Pierre-Jean Panteix[1], Laure Martinelli[2], Sabah Ben Lagha[3], Michel Vilasi[1]

[1] *Université de Lorraine, CNRS, IJL, F-54000 Nancy, FRANCE.*

[2] *CEA, Université Paris-Saclay, Den-Service de la Corrosion et du Comportement des Matériaux dans leur Environnement (SCCME), F-91191, Gif-sur-Yvette, FRANCE.*

[3] *AREVA NC, Tour Areva, 1 Place Jean Millier, F-92084, Paris-La-Défense Cedex, FRANCE*

*corresponding author, now at [2]
e-mail: eric.schmucker@cea.fr; phone: + 33 (0) 1 69 08 50 20

Abstract

The relationship between the corrosion behavior of a Ni-30Cr alloy and the physicochemical properties of chromium in silicate and borosilicate melts at 1150°C has been investigated. Three glass compositions have been chosen in order to identify the effect of basicity and viscosity. The chromium solubility limits in borosilicate melts have been determined and compared with the basicity of the melts. The chromium diffusion coefficients in the melts have been determined with the square-wave voltammetry method. A strong impact of the melt viscosity has been found on the corrosion behavior of the Ni-30Cr alloy. This dependency indicates a mechanism involving a diffusion-limited process for the dissolution of the oxide.

Keywords: Silicate melts; Solubility; Diffusion; Electrochemistry; Corrosion

1. Introduction

Nickel-based alloys with a high chromium content offer useful properties for high temperature applications involving a metallic material in contact with a glass melt, e.g. for nuclear wastes vitrification [1] or glass fiber production [2,3]. Besides their good mechanical strength at high temperature, these alloys are able to develop a Cr_2O_3 protective oxide layer when oxidized. Chromium oxide provides a suitable protection against corrosion induced by glass melts due to

the low solubility limit of chromium in silicate melts [4-6]. The stability of this Cr_2O_3 layer is therefore dependent on the physicochemical properties of the melt and of chromium in the melt. Indeed, the basicity of the melt affects the solubility of chromium. Dissolution of chromia in silicate melts has been well described by several authors with Eq. 1 to 3 [5-8]. First, the dissolution of Cr_2O_3 into Cr^{III} follows an acid base reaction:

$$\frac{1}{2}Cr_2O_{3\,(s)} + \left(x - \frac{3}{2}\right)O^{2-} \leftrightarrow Cr^{III}O_x^{(2x-3)-} \qquad \text{Equation 1}$$

Then, depending on the redox conditions, Cr^{III} can be either oxidized into Cr^{VI} or reduced into Cr^{II}:

$$Cr^{III}O_x^{(2x-3)-} + \frac{3}{4}O_2 \leftrightarrow Cr^{VI}O_y^{(2y-6)-} + \left(x - y + \frac{3}{2}\right)O^{2-} \qquad \text{Equation 2}$$

$$Cr^{III}O_x^{(2x-3)-} + \left(z - x + \frac{1}{2}\right)O^{2-} \leftrightarrow Cr^{II}O_z^{(2z-2)-} + \frac{1}{4}O_2 \qquad \text{Equation 3}$$

The presence of the basic oxide ion O^{2-} in Eq. 1 to 3 evidences the role of the melt basicity on the dissolution process of chromium in glass melts. Besides, a decreasing melt viscosity can lead to a faster diffusion of dissolved elements in the melt and may result in an accelerated corrosion rate, as it is the case for ceramic refractories [9]. Different studies have been focused on the effect of the melt basicity on the corrosion behavior of chromia-forming materials [10-12]. In the Na_2O-SiO_2 system, the increase of the corrosion rate of pure chromium with the melt basicity has been attributed to the increase of the Cr^{VI} solubility limit [10]. However, in these studies, the possible effect of viscosity has not been taken into consideration. Indeed, the more basic the glass is, the more depolymerized it is, with a low viscosity allowing a rapid diffusion in the melt, as illustrated by the value of diffusion coefficients of some elements in Na_2O-$xSiO_2$ melts by Von der Gönna and Rüssel [13,14].

As a consequence, in this paper, the corrosion behavior of a binary Ni-30Cr alloy in three different glass melts has been studied at 1150°C with immersion tests and electrochemical measurements. In addition, the physicochemical properties of chromium in these glass melts, *i.e.* solubility limits and diffusion coefficients, have been determined. Eventually, a focus is made on the relationship between both the diffusion coefficients and solubility limits of chromium in the glass melts and the corrosion behavior of the alloy in these media.

2. Materials and methods

2.1. Alloy and glasses compositions

The synthesis and characterization of the Ni-30Cr (wt.%) alloy used for corrosion tests is described in a previous paper [15]. The composition of the alloy was assessed by EDX measurements and the Cr content is 30.5±1.2 wt.%. The microstructure of the alloy presents coarse grains of several hundred of micrometers. Rod-shaped samples were prepared by electro-erosion with a 25 mm length and a 5.5 mm diameter. The surface of the samples was then ground with a P1200 SiC paper and ultrasonically cleaned in ethanol.

Glasses were synthesized by the Cerfav (Centre Européen de Recherches et de Formation aux Arts Verriers) by mixing Na_2CO_3, H_3BO_3 and SiO_2 powders, and heating at high temperature. The compositions and properties of the three glasses used in this study are listed in Table 1. Glass compositions have been measured by EPMA with the analysis conditions listed in Table 2. Viscosity data are taken from experimental characterizations [16,17] when available, or calculated with the statistical model given by Fluegel *et al.* [18] or with Factsage software [19]. The optical basicity is considered as the basicity scale in this paper [20]. The optical basicity of glasses is calculated with Eq. 4:

$$\Lambda_{\text{glass}} = \sum_{\text{i}} X_{\text{i}} \Lambda_{(\text{oxide i})} \qquad \text{Equation 4}$$

where Λ (unit less) represents the optical basicity and X_{i} is the equivalent molar fraction of oxygen, *i.e.* the number of oxygen atoms brought by the oxide i on the total number of oxygen atoms in the glass composition.

N3S (Na_2O-$3SiO_2$) and 2.3NB5S ($2.3Na_2O$-B_2O_3-$5SiO_2$) glass compositions have same optical basicity and very different viscosity whereas the 0.75NB2.75S ($0.75Na_2O$-B_2O_3-$2.75SiO_2$) composition has a similar low viscosity to that of 2.3NB5S but is more acidic. Furthermore, at the temperature of 1150°C, all these glass compositions are in a single-phased liquid state.

2.2. Corrosion tests

For corrosion tests of Ni-30Cr by simple immersion in silicate melts, Ni-30Cr samples were mounted in refractory mullite tubes and sealed with alumina cement (Resbond 989FS). Samples were then immersed in about 800 g of glass contained in a Pt-10%Rh crucible placed in a muffle furnace in laboratory air. Prior to immersion, Ni-30Cr samples were preoxidized in laboratory air above the glass batch for 2 h at 1150°C in order to develop an initial Cr_2O_3 layer. The thickness of this preoxidation layer is about 2.6 to 4.4 µm (Fig. 1). Cross-sectional SEM observations were performed with a JEOL J7600F apparatus in BSE contrast mode.

2.3. Electrochemistry

Anodic polarization experiments were performed on Ni-30Cr samples immersed in the silicate melts in order to determine if a passivation domain can exist. Therefore, a three-electrode device was used for that purpose with Ni-30Cr rod as working electrode, yttria stabilized zirconia rod as reference electrode and a platinum plate as counter-electrode. A potential increase was imposed from -20 mV *vs.* open circuit potential up to +500 mV *vs.* ZrO_2 with a scan rate of 1

mV s^{-1}. For the anodic polarization experiments, no preoxidation treatment was performed on the samples. More detailed information about the device and apparatus can be found in reference [2].

A similar three-electrode device was also used for the determination of chromium diffusion coefficient in silicate melts with the aid of square-wave voltammetry, using a platinum wire as working electrode (length: 12 mm, diameter: 0.5 mm). After an initial polarization for 2 seconds at the starting potential, the voltammograms were recorded in the cathodic direction from +100 mV down to -1200 mV *vs* ZrO_2 in each raw glass or glass doped with 0.83 wt.% Cr_2O_3. Scanning was performed with a potential amplitude ΔE_{sw} of 100 mV, a potential step ΔE_s of 1 mV and square wave frequencies f ranging from 2 up to 1000 Hz (Fig. 2).

In order to isolate the current due to the electrochemical response of chromium from the matrix current, square wave voltammograms were first recorded in each raw glass melt (blank measurement) and then in each melt doped with 0.83 wt.% Cr_2O_3. Using the square wave voltammetry technique, the differential peak current response (ΔI_p) imputed to a reversible electrochemical reaction can be linked to the diffusion coefficient of the reactive species by the following equation [22,23]:

$$\frac{\Delta I_p \sqrt{\pi}}{nFAC_0\sqrt{2fD}} = \varphi_p\left(1.21 + \frac{\Delta E_s}{2\Delta E_{sw}}\right) \qquad \text{Equation 5}$$

with

$$\varphi_p = \frac{\sqrt{\xi} - 1}{\sqrt{\xi} + 1} \qquad \text{Equation 6}$$

and

$$\xi = \exp\left[\frac{nF(E - E_{1/2})}{RT}\right] \qquad \text{Equation 7}$$

where ΔI_p is the peak current in A, n is the number of electrons exchanged in the electrochemical process, F is the Faraday constant in C mol^{-1}, A is the surface of the electrode, which is here equal to 0.385 cm^2 (± 10%), D is the diffusion coefficient of the reactive species in cm^2 s^{-1}, C_0 is its initial concentration in the melt in mol cm^{-3}, ΔE_s is the potential step and ΔE_{sw} is the potential amplitude of the square wave in V, f is the scanning frequency in Hz, $E_{1/2}$ is the half-wave potential of the redox reaction in V, R is the ideal gas constant in J K^{-1} mol^{-1} and T is the absolute temperature in K.

2.4. Chromium solubility limit measurements

The chromium solubility limits in the silicate melts were determined thanks to a specific closed reactor allowing the control of temperature, oxygen fugacity and melt composition. The sample consists of a small glass ball (about 100 mg) mixed with Cr_2O_3 powder. High temperature treatments were performed at 1150°C in oxygen atmosphere ranging from 3.10^{-13} atm up to 0.2 atm (or 3.10^{-8} to 2.10^{4} Pa). The oxygen pressures are imposed by metal/oxide buffers. Technical details about this device, sample preparation and chromium chemistry in glass melts are given in references [6,24]. Chromium contents in the Cr-saturated glassy matrix were then measured with an SX100 Electron Probe Micro-Analyzer with a 15 kV acceleration voltage. EPMA analysis conditions are reported in Table 2.

3. Results

3.1. Corrosion behavior of Ni-30Cr in silicate melts

3.1.1. Linear anodic polarization

Linear anodic polarization curves of the as-polished Ni-30Cr alloy immersed in the glass melts are shown in Fig. 3. Polarization curves in the N3S and 0.75NB2.75S melts show a plateau with a relatively low current density, typical of the passivation state of a chromia-forming alloy in silicate melts at high temperature [2,3,25]. Thanks to previous studies establishing a redox potential scale in glass melts, the shape of the polarization curves can be explained as follows [2,25]: starting from low potentials, the increase of current density corresponds to the oxidation of metallic chromium (Cr^0) into Cr^{II} species. In addition, the corrosion potential (at i = 0 mA cm^{-2}) of the alloy is similar in the two borosilicate melts and lower than in the binary N3S melt. In the N3S and 0.75NB2.75S glass melts, a strong current density decrease is observed for potentials superior to about -900 mV. The establishment of such passivation plateau is attributed to the oxidation of Cr^{II} into Cr^{III} giving rise to the formation of a Cr_2O_3 layer at the surface of the substrate. This layer limits the electrochemical interactions between the alloy and the melt, and thus decreases the current density. Moreover, the minimum current density is equivalent, about 1-2 mA cm^{-2}, in these two melts. However, the passivation plateau in the N3S melt exhibits a wider potential range than the one in 0.75NB2.75S. In the 2.3NB5S melt, no passivation of the alloy is achieved and the current density remains above 13 mA cm^{-2}. The peak starting around -400 mV can be attributed to the oxidation of Ni^{II} into Ni^{III} – since oxidation of Ni^0 into Ni^{II} occurs at a potential close to the Cr^{III}/Cr^{II} redox potential – in agreement with the potential scale from previous works [25]. The absence of this Ni^{III}/Ni^{II} oxidation peak on the polarization curves in N3S and 0.75NB2.75S melts can be attributed to the presence of the Cr_2O_3 passive layer which hinders any further oxidation of nickel from the

alloy. Eventually at higher potentials, the increase of current density after the passivation domain is attributed to the oxidation of Cr^{III} into Cr^{VI} and the loss of the protective Cr_2O_3 scale.

3.1.2. Immersion tests of preoxidized Ni-30Cr

After quenching in air, a greenish coloration of the glass surrounding the alloy rods has been observed in all glasses. This coloration is a typical witness of the presence of Cr^{III} ions in the glass [26]. Cross-sections of the preoxidized Ni-30Cr alloy immersed in the glass melts at 1150°C are presented in Fig. 4. After 25 h of immersion in the N3S melt (Fig. 4a), an 11 µm thick, adherent and homogenous oxide layer is present at the surface of the alloy. EDX measurements have confirmed that the composition of this oxide layer corresponds to Cr_2O_3 with only traces of nickel (less than 1 at.%). Thus, compared to its initial thickness of about 2.3 to 4.4 µm (Fig. 1), a substantial Cr_2O_3 growth occurred. In the 0.75NB2.75S melt, the thickness of the Cr_2O_3 layer after 25 h of immersion is only about 5-6 µm, indicating a lower growth rate in this glass composition (Fig. 4b). However, after a short immersion of 2 h 30 in the 2.3NB5S melt, the initial oxide has been entirely dissolved in the melt and the cross-section shows a strongly corroded surface of the alloy with glass penetration along the grain boundaries of the alloy, internal oxidation of the alloy within a few micrometers and some corrosion products in the melt, in the vicinity of the alloy (Fig. 4c). These corrosion products have been identified as mixed nickel-chromium oxide by EDX measurements. Cross-sections observations thus indicate that the dissolution rate of the oxide layer is higher (resp. lower) than its formation rate in the 2.3NB5S (resp. N3S and 0.75NB2.75S) melt, in agreement with the absence (resp. presence) of a passivation domain on the anodic polarization curves (Fig. 3).

3.2. Chromium solubility limit in the melts

First of all, the chromium solubility limits in the N3S melt at 1150°C were extrapolated from the data obtained by Khedim *et al.* [5]. These authors gave solubility limit values at 1175°C, 1200°C and 1250°C. Chromium solubility limits in the N3S melt were extrapolated with an Arrhenius law for each redox buffer and results are shown in Table 3. For the borosilicate melts, experiments have been performed with several durations (30 min, 1 h and 2 h) and have revealed that 1 h of treatment at 1150°C was sufficient to reach the thermodynamic equilibrium. The achievement of thermodynamic equilibrium is considered when the chromium content dissolved in the glass matrix is the same on the edge and in the core of the sample, and when this content does not vary with the heat treatment duration [8]. The results obtained in the borosilicate melts after 1 h at 1150°C in oxygen atmospheres ranging from 3.10^{-13} up to 0.2 atm are reported in Table 3. The chromium solubility limits are represented in Fig. 5 as a function of the oxygen fugacity for the different melts. For each glass melt, the minimum chromium solubility limit is found in the $-10 < \log f(O_2) < -2$ region. In this $f(O_2)$ domain, the predominant

redox state for chromium is Cr^{III} [7]. In oxidizing conditions (log $f(O_2)$ > -2), the stabilization of Cr^{VI} species occurs while in reducing conditions (log $f(O_2)$ < -10), the formation of Cr^{II} species is favored [7]. Considering Fig. 5, it clearly appears that the chromium solubility limits are very similar in the N3S and 2.3NB5S melts which have the same optical basicity. The 0.75NB2.75S melt, which is more acidic, exhibits lower solubility limits all over the $f(O_2)$ range. Furthermore, these solubility limit curves can be fitted with the following equation:

$$S_{\mathrm{Cr}}(\mathrm{at.\,\%}) = A + B f_{O_2}^{-1/4} + C f_{O_2}^{3/4} \qquad \text{Equation 8}$$

Eq. 8 was given by Khedim *et al.* [5] and represents the total amount of dissolved chromium (Cr^{II} + Cr^{III} + Cr^{VI}) in the melt as a function of the oxygen fugacity. The parameters *A*, *B* and *C* have been adjusted with the experimental data thanks to the Origin software. *A* represents the minimum chromium solubility limit, corresponding to the Cr^{III} solubility limit. The second and the third terms of Eq. 8 are respectively associated to Cr^{II} and Cr^{VI} species.

3.3. Chromium diffusion coefficient in the melts

Square wave voltammetry method has been used to determine the diffusion coefficient of chromium species in glass melts. The voltammograms recorded in the cathodic direction in the Cr-doped N3S melt are represented on Fig. 6. The current density response increases with increasing scanning frequency. The subtraction of the matrix signal – obtained with the same experimental conditions in the raw N3S melt – to the Cr-doped N3S signal gives the electrochemical response associated to the reduction of Cr species only, as shown for instance in Fig. 7a. From Fig. 7a, the redox potential of the Cr^{VI}/Cr^{III} and Cr^{III}/Cr^{II} couples in the N3S melt at 1150°C can be read and are respectively equal to about -30 mV and -840 mV. These values are in agreement with data from the literature for different glass compositions, ranging from -120 mV up to 30 mV and from -880 mV up to -650 mV respectively, for temperatures above 1000°C [2,13,14,27].

The dependence of the Cr^{III}/Cr^{II} reduction peak current in the N3S melt versus the square root of the scanning frequency is shown on Fig. 8a. A linear dependence is found when the electrochemical system is reversible. In the present case, the linear dependency is found for scanning frequencies inferior to 100 Hz. Therefore, thanks to Eq. 5 and the slope of the linear part of the curve in Fig. 8a, the diffusion coefficient of Cr^{III} in the N3S melt at 1150°C can be calculated and is equal to 1.4 x 10^{-7} cm^2 s^{-1}.

The same procedure has been applied to the two borosilicate compositions in order to determine the diffusion coefficient of Cr^{III}. Examples of Cr-doped melt and matrix current subtraction for the borosilicate melts are shown in Fig. 7b and c. The redox potentials of the Cr^{VI}/Cr^{III} couple are equal to about -100 mV and -80 mV in the 2.3NB5S and the 0.75NB2.75S melts respectively, while the redox potentials of the Cr^{III}/Cr^{II} couple are respectively equal to about -930 mV and -910 mV. The corresponding Cr^{III}/Cr^{II} reduction peak current dependencies versus the square root of the scanning frequency are shown in Fig. 8b and c. The linearity domain

between ΔI_p and $\sqrt{f}$ for the 2.3NB5S melt extends up to 25 Hz while it only extends up to a very low value of 5 Hz in the 0.75NB2.75S melt. Differential voltammograms in 2.3NB5S melts are reported in Fig. 9 for different scanning frequencies. From Fig. 9, it is clearly visible that the Cr^{III}/Cr^{II} reduction peak potential is constant near -930 mV at low frequencies while a peak shift is observed for higher frequencies starting from 25 Hz. A peak potential shift with scanning frequency is typical for an irreversible reaction, *i.e.* a slow charge transfer [28]. These observations are consistent with the linearity domain obtained on the ΔI_p *vs.* $\sqrt{f}$ graph that has been attributed to the reversibility domain of the electrochemical reaction. Therefore, the diffusion coefficients of Cr^{III} in the 2.3NB5S and in the 0.75NB2.75S, calculated with Eq. 5 are respectively equal to 5.0×10^{-6} and 1.5×10^{-6} cm^2 s^{-1}.

Moreover, a similar procedure has been carried out in order to determine the diffusion coefficients of Cr^{VI} in these melts, as well as the diffusion coefficients of Cr^{II}. For this latter, the potential scanning has been carried out in the anodic direction, starting from -1000 mV up to 100 mV. Results about the chromium diffusion coefficients in these glass melts are summarized in Table 4.

4. Discussion

4.1. Melt basicity - chromium solubility relationship

In the present study, the chromium solubility limit has been found to be lower in the more acidic glass melt whatever the oxidation state of chromium is. This result was expected for the Cr^{VI} species which are stabilized by the formation of tetra-coordinated chromate complexes CrO_4^{2-} [29,30] and whose solubility limits are therefore higher when the basicity, *i.e.* the free oxygen ion O^{2-} activity, increases in soda-silica and soda-lime silicate melts [5,6]. However, only a decrease of the solubility limits of Cr^{II} and Cr^{III} species when the melt basicity increases has been observed until now, in binary sodium silicate and ternary soda-lime silicate [5,6].

In addition, identical chromium solubility limits have been found in the N3S and the 2.3NB5S melt which have the same optical basicity. This result is in contrast with those obtained by Khedim [5,6] and Abdullah [32], who observed lower chromium solubility limits in ternary Na_2O-CaO-SiO_2 systems compared to binary Na_2O-SiO_2 systems with equivalent optical basicity. This different behavior may be explained by the different structural role adopted by the third oxide component (boron or calcium oxide). Indeed, B_2O_3 is a network former like SiO_2, whereas CaO acts like a network modifier like Na_2O. The disparity between solubility in soda-silica and soda-lime-silica systems may lie in the different valence states of the sodium and calcium ions and therefore their structural environment as well.

These unexpected results can be the consequence of the peculiar atomic structure of borosilicate glasses which exhibits a non-linear and non-monotonic variation with their composition. Indeed, boron entities can either be in trigonal configuration or in tetragonal configuration

depending on the Na_2O/B_2O_3 and SiO_2/B_2O_3 molar ratios [31]. At high temperature, in high soda NBS systems, sodium might be more likely to create non-bridging oxygen atoms [31,33] just as in binary soda-silica melts, explaining the similar chromium solubility limits in the N3S and 2.3NB5S melts.

Since the calculation of the optical basicity of a glass is a simplistic model described by the weighted sum of the basicity of pure oxides, the limits of this model may appear when those oxides are introduced in a complex silicate network, making the comparison between melt systems of different nature abstruse. Further characterizations on the high temperature structure of these glass melts and on how these structures (e.g. trigonal or tetragonal boron units) affect the chromium coordination are then required. Spectroscopic methods could give useful information like the glass melt structures and the chromium coordination in these borosilicate melts.

4.2. Melt viscosity - chromium diffusion relationship

The diffusion coefficient for Cr^{II}, Cr^{III} and Cr^{VI} in the three glass melts have been plotted in Fig. 10 versus the melt viscosities, as well as data from the literature [13,14,34-36]. Viscosities of the melts taken from literature have been calculated with the statistical model from Fluegel *et al.* [18]. A linear regression on all these values of $D(Cr^{III})$ and $D(Cr^{VI})$ gives a direct dependence of the Cr^{III} and Cr^{VI} diffusion coefficients as a function of the inverse of the melt viscosity. Such dependence is expected for atomic diffusion in liquid media [37-40].

Furthermore, it appears that the diffusion coefficients of Cr^{II} and Cr^{III} species are very similar, while the diffusion coefficients for Cr^{VI} are about two orders of magnitude lower. These findings seems logical given that Cr^{III} and Cr^{II} have a close valence and a similar chemical environment which is a coordination sphere with six oxygen atoms in octahedral symmetry (distorted by Jahn-Teller effect in the case of Cr^{II}) within the glass structure [30]. On the other hand, Cr^{VI} is a highly polarized species with high valence and a coordination sphere with four oxide ions O^{2-} in a tetrahedral symmetry [29,30].

4.3. Chromium solubility/diffusion - Ni-30Cr corrosion relationship

The stability of a Cr_2O_3 layer at the alloy/melt interface is governed by the competition between its formation and its dissolution in the melt. As the Ni content in the oxide layer is very low and

corresponds to usual values of Ni doping in chromia [15], we consider that it has no effect on the dissolution of chromia. The dissolution kinetics of the oxide can be limited either by the interfacial reaction rate (*i.e.* chromium oxide solubilization) or by the mass transfer of chromium in the melt. In the latter case, the stability of the oxide layer should be dependent on the diffusion coefficient of chromium in the glass melt.

It has been evidenced that the chromium solubility limits in the N3S and 2.3NB5S melts are similar (Fig. 5 and Table 3). However, the diffusion of chromium is way faster in the 2.3NB5S borosilicate melt than in the binary N3S melt. Given that the corrosion behavior of the Ni-30Cr alloy is different in these melts, as the passivating layer is not stable in the 2.3NB5S melt, the dissolution of Cr_2O_3 is likely to be controlled by the mass transfer of chromium in the liquid phase. Therefore, the viscosity of the melt and thus the diffusion of chromium obviously have a strong impact on the corrosion behavior of the alloy. For example, in the case of N3S and 2.3NB5S melts, a decrease of the diffusion coefficient of Cr^{III} by a factor 35 leads to the establishment of a durable passive state of the Ni-30Cr alloy in the N3S melt, whereas a total dissolution of the initial Cr_2O_3 layer occurs within a few hours in the 2.3NB5S melt. For this latter melt, as no chromia layer is observed after a few hours, but Ni-Cr oxides are identified in the melt near the alloy/melt interface (Fig. 4c) and since oxidation of nickel is identified by electrochemistry (Fig. 3), oxidation of nickel will play critical a role on the global corrosion kinetics when the Cr_2O_3 layer disappears. Indeed, NiO is not a protective oxide in silicate melts due to its higher solubility in these media [2,41].

In the 0.75NB2.75S melt, the Ni-30Cr alloy stayed in the passive state for at least 25 h, but with a slower overall growth of the oxide layer compared to the growth in the N3S melt. On one hand, the solubility of Cr^{III} in 0.75NB2.75S is inferior to the solubility in the other melts by a factor 1.3 approximately. On the other hand, its diffusion coefficient is 10 times greater than in the N3S melt but about 3 times lower compared to the 2.3NB5S melt. Despite the lower Cr^{III} solubility in 0.75NB2.75S, the increase by an order of magnitude of the diffusion coefficient of Cr^{III} leads to a decrease of the overall growth rate of the Cr_2O_3 layer, compared to its behavior in N3S, demonstrating the strong impact of the melt viscosity on the corrosion behavior of chromia-forming alloys in glass melts.

5. Conclusions

In our previous studies about the corrosion of chromia-forming alloys by glass melts, focus were made on the effect of the melt basicity and the chromium solubility in order to explain the corrosion behavior. However, the influence of viscosity variations were ignored. In this paper, the corrosion behavior of a Ni-30Cr alloy in different melt compositions has been correlated to the physicochemical properties of chromium in these melts, *i.e.* its solubility and its diffusion coefficient.

A set of data concerning the chromium solubility in the borosilicate glass melts at 1150°C in atmosphere ranging from 10^{-13} up to 0.2 atm O_2 has been obtained as well as the diffusion coefficient of Cr^{II}, Cr^{III} and Cr^{VI} species in three different melt compositions at 1150°C. The solubility limits of chromium are identical in the N3S and 2.3NB5S which have the same basicity. In the acidic 0.75NB2.75S melt, the solubility limits are lower whatever the fO_2. Square wave voltammetry measurements have evidenced that higher diffusion coefficient of chromium have been found in the melts with the lowest viscosities.

These data were used to explain the different corrosion behaviors of Ni-30Cr alloy in the glass melts studied here. Thanks to the immersion tests of preoxidized Ni-30Cr samples, it has been shown that a low viscosity of the melt, and thus a high diffusion coefficient, strongly compromises the stability of the protective Cr_2O_3 layer. This finding also evidences that the mechanism governing the dissolution of the oxide is kinetically limited by the diffusion of chromium in the melt.

References

[1] P. Sengupta, Interaction study between nuclear waste-glass melt and ceramic melter bellow liner materials, J. Nucl. Mater. 411 (2011) 181-184.

[2] J. Di Martino, C. Rapin, P. Berthod, R. Podor, P. Steinmetz, Corrosion of metals and alloys in molten glasses. Part 1: glass electrochemical properties and pure metal (Fe, Co, Ni, Cr) behaviours, Corros. Sci. 46 (2004) 1849-1864.

[3] J. Di Martino, C. Rapin, P. Berthod, R. Podor, P. Steinmetz, Corrosion of metals and alloys in molten glasses. Part 2: nickel and cobalt high chromium superalloys behaviour and protection, Corros. Sci. 46 (2004) 1865-1881.

[4] C.W. Kim, K. Choi, J.K. Park, S.W. Shin, M.J. Song, Enthalpies of Chromium Oxide Solution in Soda Lime Borosilicate Glass Systems, J. Am. Ceram. Soc. 84 (2001) 2987-2990.

[5] H. Khedim, R. Podor, P.J. Panteix, C. Rapin, M. Vilasi, Solubility of chromium oxide in binary soda-silicate melts, J. Non-Cryst. Solids 356 (2010) 2734-2741.

[6] H. Khedim, T. Katrina, R. Podor, P.J. Panteix, C. Rapin, M. Vilasi, Solubility of Cr_2O_3 and Speciation of Chromium in Soda-Lime-Silicate Melts, J. Am. Ceram. Soc. 93 (2010) 1347-1354.

[7] H. Khedim, R. Podor, C. Rapin, M. Vilasi, Redox-Control Solubility Oxide in Soda-Silicate Melts, J. Am. Ceram. Soc. 91 (2008) 3571-3579.

[8] T.K. Abdullah, C. Petitjean, P.J. Panteix, C. Rapin, M. Vilasi, Z. Hussain, A.A. Rahim, Dissolution equilibrium of chromium oxide in a soda lime silicate melt exposed to oxidizing and reducing atmospheres, Mater. Chem. Phys. 142 (2013) 572-579.

[9] P.A Bingham, R.J. Hand, Corrosion of glass contact refractories for the vitrification of radioactive wastes: a review, Int. Mater. Rev. 56 (2011) 226-242.

[10] S. Abdelouhab, C. Rapin, R. Podor, P. Berthod, M. Vilasi, Electrochemical study of chromium corrosion in Na_2O-xSiO_2 melts, J. Electrochem. Soc. 154 (2007) 500-507.

[11] H. Khedim, S. Abdelouhab, R. Podor, C. Rapin, M .Vilasi, Relationship between chromia solubility and superalloy corrosion in silicate melts – A first attempt, Mater. Sci. Forum 595 (2008) 621-627.

[12] T.K. Abdullah, C. Petitjean, P.J. Panteix, E. Schmucker, C. Rapin, M. Vilasi, Corrosion of Pure Cr and Ni-30Cr Alloy by Soda-Lime-Silicate Melts: Study of Simplified Systems, Oxid. Met. 85 (2016) 3-16.

[13] G. von der Gönna, C. Rüssel, Diffusivities of polyvalent elements in a $15Na_2O$-$85SiO_2$ glass melt, J. Non-Cryst. Solids 272 (2000) 139-146.

[14] G. von der Gönna, C. Rüssel, Diffusivities of various polyvalent elements in a Na_2O-$2SiO_2$ glass melt, J. Non-Cryst. Solids 261 (2000) 204-210.

[15] E. Schmucker, C. Petitjean, L. Martinelli, P.J. Panteix, S. Ben Lagha, M. Vilasi, Oxidation of Ni-Cr alloy at intermediate oxygen pressures. I. Diffusion mechanisms through the oxide layer, Corros. Sci. 111 (2016) 474-485.

[16] K.D. Kim, Sintering-viscosity relation for mixed-alkali glass powder compacts, J. Mater. Res. 10 (1995) 1846-1849.

[17] M.J. Pascual, A. Duran, L. Pascual, Viscosity and thermal properties of glasses in the system R_2O-B_2O_3-SiO_2, R= Li, K, Na, Phys. Chem. Glasses 43 (2002) 25-31.

[18] A. Fluegel, Glass viscosity calculation based in a global statistical modeling approach, Glass. Technol. Part A, 48 (2007) 13-30.

[19] C.W. Bale, P. Chartrand, S.A. Degterov, G. Eriksson, K. Hack, R. Ben Mahfoud, J. Melançon, A.D. Pelton, S. Peterson, FactSage thermochemical software and databases, Calphad, 26 (2002) 189-228.

[20] J.A. Duffy, A review of optical basicity and its applications to oxidic systems, Geochim. Cosmochim. Acta, 57 (1993) 3961-3970.

[21] A. Fluegel, D.A. Earl, A.K. Varshneya, T.P. Seward, Density and thermal expansion calculation of silicate glass melts from 1000°C to 1400°C, Phys. Chem. Glasses B 49 (2008) 245-257.

[22] D. Krulic, N. Fatouros, M.M. El Belamachi, Stepped potential voltammetries at stationary electrodes. Part 1. Differential staircase, differential pulse and square-wave voltammetries, J. Electroanal. Chem. 385 (1995) 33-38.

[23] N. Larabi (2005) Cinétique électrochimique du système Ti(IV)/Ti(III) dans différents milieu acides – Electroanalyse de Ti(IV). Université Pierre et Marie Curie thesis, Paris.

[24] R. Mathieu, H. Khedim, G. Libourel, R. Podor, L. Tissandier, E. Deloule, F. Faure, C. Rapin, M. Vilasi, Control of alkali-metal oxide activity in molten silicates, J. Non-Cryst. Solids 354 (2008) 2079-5083.

[25] C. Petitjean, P.J. Panteix, C. Rapin, M. Vilasi, R. Podor, Electrochemical behavior of glass melts: application to corrosion processes, Proc. Mater. Sci. 7 (2014) 101-110.

[26] O. Villain, L. Galoisy, G. Calas, Spectroscopic and structural properties of Cr^{3+} in silicate glasses: Cr^{3+} does not probe the average glass structure, J. Non-Cryst. Solids 356 (2010) 2228-2234.

[27] J.Y. Tilquin, P. Duveiller, J. Glibert, P. Claes, Effect of basicity on redox equilibria in sodium silicate melts: An in situ electrochemical investigation, J. Non-Cryst. Solids, 211 (1997) 98-104.

[28] J.J. O'Dea, J. Osteryoung, R.A. Osteryoung, Theory of Square Wave Voltammetry for Kinetic Systems, Anal. Chem. 53 (1981) 695-701.

[29] O. Villain (2009), Contribution à l'étude de l'environnement structural du chrome dans les verres, Université Pierre et Marie Curie thesis, Paris.

[30] H.D. Schreiber, L.A. Haskin, Chromium in basalts: Experimental determination of redox states and partitioning among synthetic silicate phases, Proc. Lunar. Sci. Conf. 7 (1976) 1221-1259.

[31] W.J. Dell, P.J. Bray, S.Z. Xiao, 11B NMR studies and structural modeling of Na_2O-B_2O_3-SiO_2 glasses of high soda content, J. Non-Cryst. Solids 27 (1978) 363-380.

[32] T.K. Abdullah, C. Petitjean, P.J. Panteix, C. Rapin, M. Vilasi, Z. Hussain, A.A. Rahim, Stability of Protective Oxide Layer Against Corrosion: Solubility Measurements of Chromium in Soda Lime Silicate Melts, Oxid. Met. 80 (2013) 611-622.

[33] L. Cormier, O. Majérus, D.R. Neuvillle, G. Calas, Temperature-induced structural modifications between alkali borate glasses and melts, J. Am. Ceram. Soc. 89 (2006) 13-19.

[34] O. Claussen, C. Rüssel, Diffusivities of polyvalent elements in glass melts, Solid State Ionics, 105 (1998) 289-296.

[35] O. Claussen, S. Gerlach, C. Rüssel, Self-diffusivity of polyvalent ions in silicate liquids, J. Non-Cryst. Solids 253 (1999) 76-83.

[36] J. Vondrak, D. Rohanova, B. Klapste, J. Velicak, Voltammetric measurements of the Pt electrode capacity and the determination of the polyvalent ions diffusion coefficients in the glass melt, Ceram.-Silik. 47 (2003) 51-55.

[37] H. Eyring, Viscosity, plasticity and diffusion as examples of absolute reaction rates, J. Chem. Phys. 4 (1936) 283.

[38] A. Einstein, Über die von der molecular-kinetischen Theorie der Wärme geforderte Bewegung von in ruhenden Flüssigkeiten suspendierten Teilchen, Ann. Phys. 17 (1905) 549-560.

[39] Y. Oishi, R. Terai, H. Ueda, Oxygen Diffusion in Liquid Silicates and Relation to their Viscosity, in Mass Transport Phenomena in Ceramics, ed. A. Cooper and A. Heuer, Plenum Press, New-York, 297-310.

[40] C.E. Lesher, R.L. Hervig, D. Tinker, Self diffusion of network fomers (silicon and oxygen) in naturally occurring basaltic liquid, Geochim. Cosmochim. Acta 60 (1996) 405-413.

[41] L.J Manfredo, R.N. McNally, Solubility of Refractory Oxides in Soda-Lime Glass, J. Am. Ceram. Soc. 67 (1984) 155-158.

Table 1: Theoretical and measured compositions (mol.%) and physicochemical properties of the glasses at 1150°C. Standard deviations are given as uncertainty.

		N3S	2.3NB5S	0.75NB2.75S
Na_2O	th.	25	28	16.69
	exp.	23.30 ± 0.31	26.28 ± 0.39	16.78 ± 0.23
B_2O_3	th.	-	12	22.23
	exp.	-	13.11 ± 0.30	22.54 ± 0.54
SiO_2	th.	75	60	61.08
	exp.	76.70 ± 0.14	60.61 ± 0.54	60.68 ± 0.54
Optical basicity (Λ) [20]		0.57	0.56	0.52
Viscosity (log η(dPa s))		2,89 - 2,97 [16,18,19]	1,42* [18] 1,98 [19]	1,57 [17] 2,09 [19]
Density ρ (g cm^{-3}) [21]		2.24	2.20	2.17

*glass composition is slightly outside the model range proposed by [18]

Table 2: Glass analysis conditions with EPMA

Element	Standard	Current	Counting time (peak)	Counting time (background)
Cr	Cr_2O_3	10 nA	10 s	5 s
Al	Albite $NaAlSi_2O_8$			
Si				
Na				
B	Danburite $CaB_2Si_2O_8$	30 nA	30 s	15 s
O	Calculated by stoichiometry			

Figure 1: BSE micrograph of the oxide layer formed on Ni-30Cr alloy after preoxidation at 1150°C during 2 h.

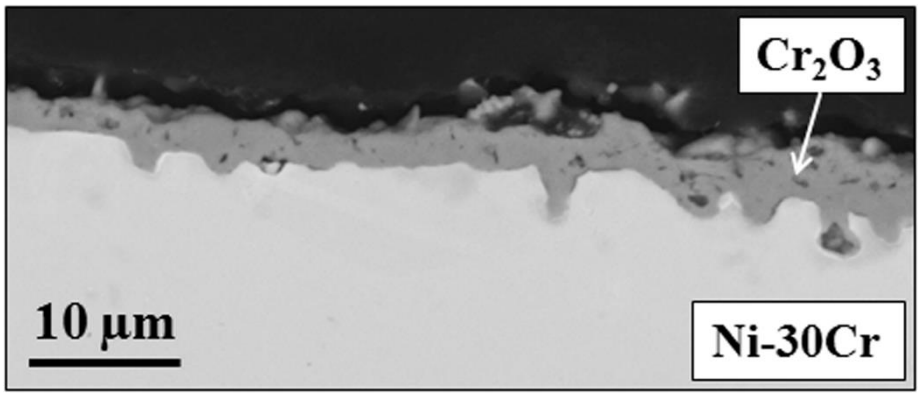

Figure 2: Square wave waveform showing the electrochemical parameters ΔE_s, ΔE_{sw} and f.

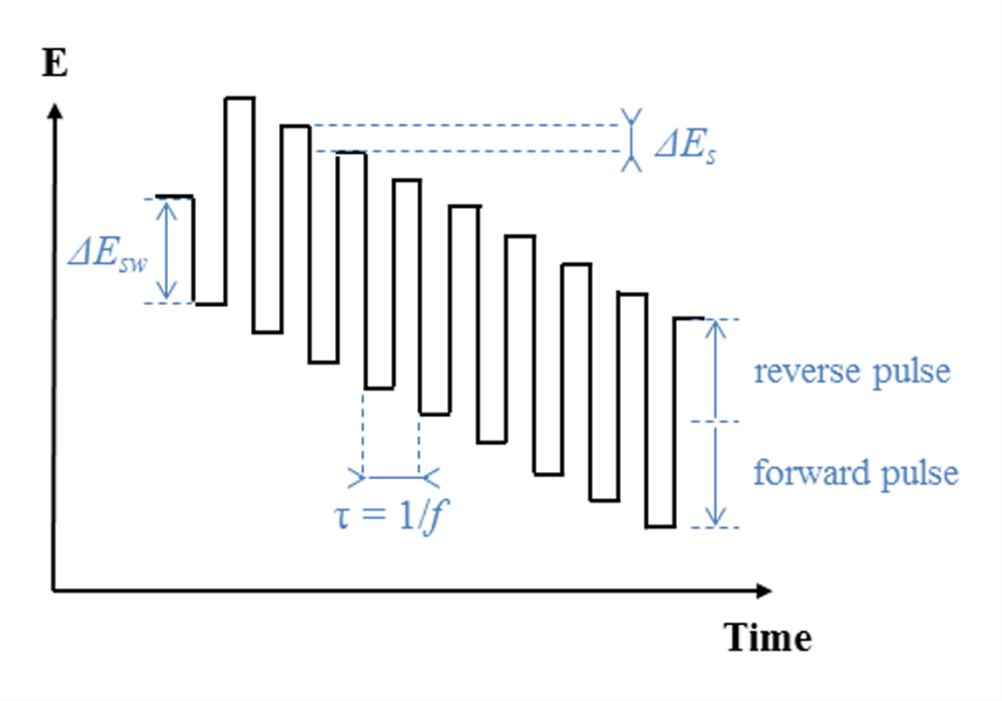

Figure 3: Anodic polarization curves of Ni-30Cr alloy at 1150°C in the glass melts (scan rate = 1 mV s^{-1}).

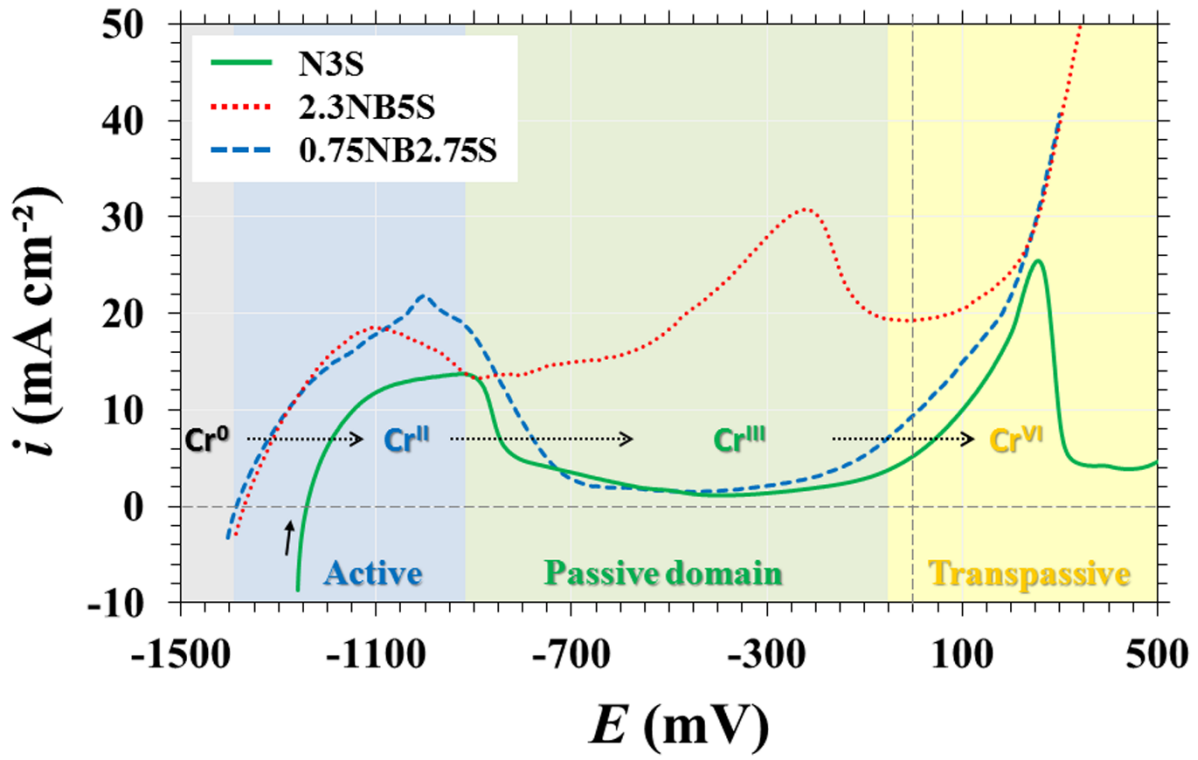

Figure 4: Cross-section BSE micrographs of the Ni-30Cr/glass melt interface after immersion at 1150°C in (a) N3S melt during 25 h; (b) 0.75NB2.75S melt during 25 h and (c) 2.3NB5S during 2 h 30.

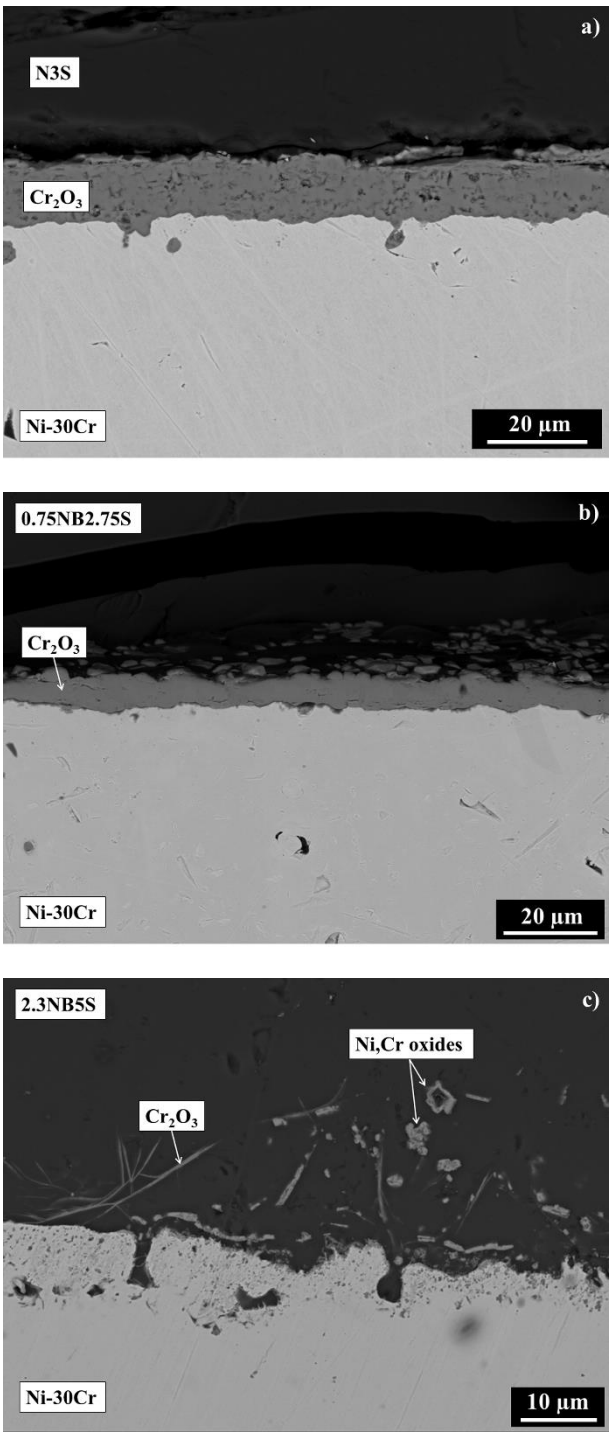

Figure 5: Chromium solubility limits in the glass melts as a function of the oxygen fugacity at 1150°C.

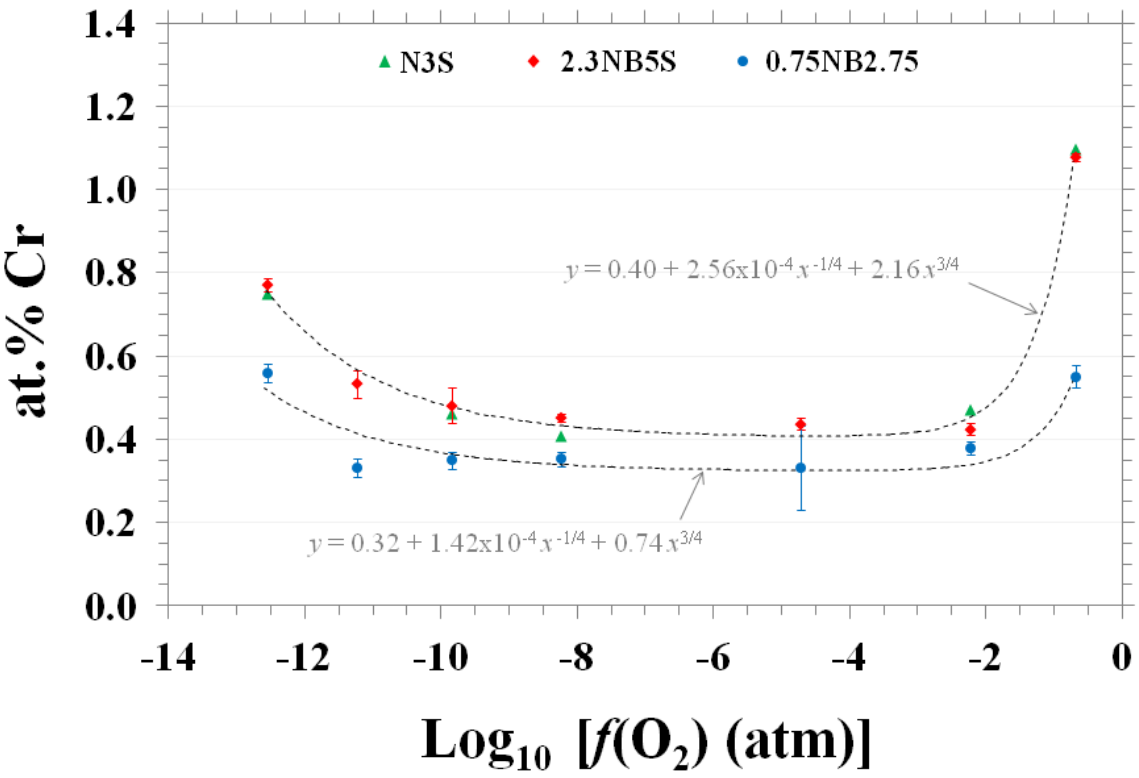

Figure 6: Square wave voltammograms of the Cr-doped N3S melt at 1150°C for various square wave frequencies. Scanning is carried out from anodic to cathodic potentials.

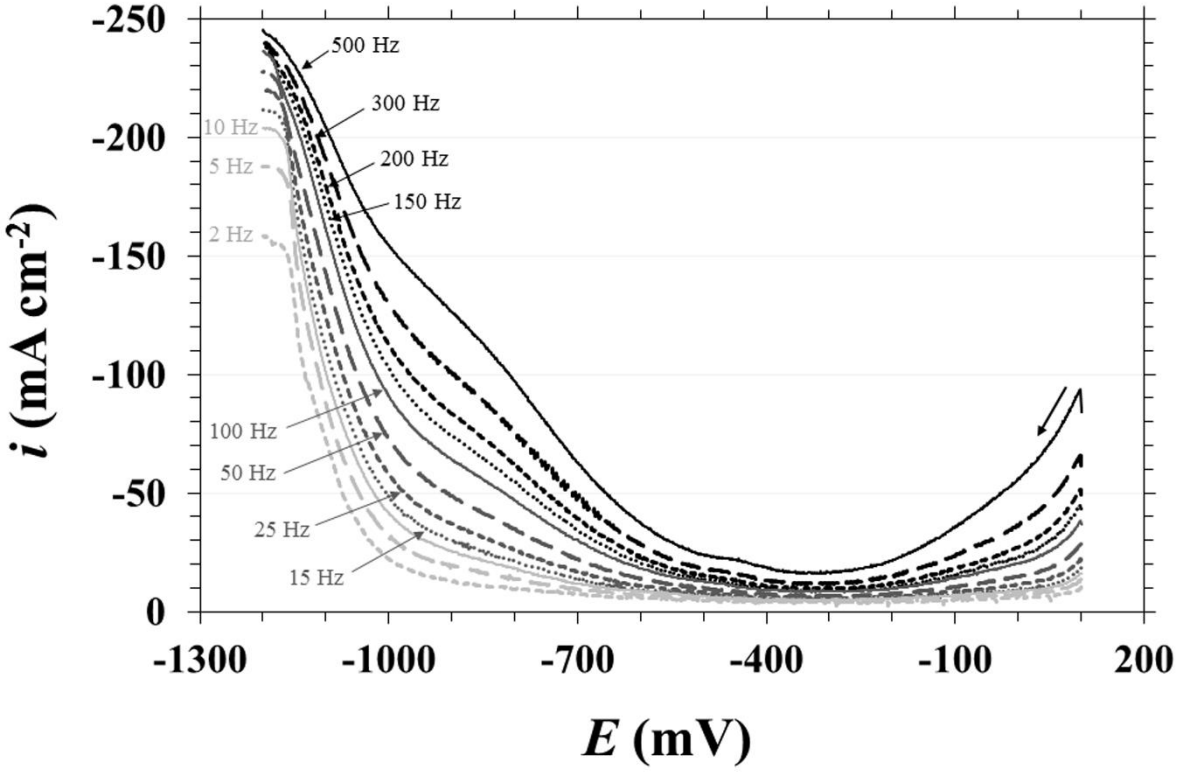

Figure 7: Square wave voltammograms of the Cr-doped melts (solid line), the Cr-free melts (dashed line) and their difference (dotted line) at 1150°C in (a) N3S melt (ΔE_{sw} = 100 mV; f = 100 Hz); (b) 2.3NB5S melt (ΔE_{sw} = 100 mV; f = 15 Hz) and (c) 0.75NB2.75S melt (ΔE_{sw} = 100 mV; f = 2 Hz). Scanning is carried out from anodic to cathodic potentials.

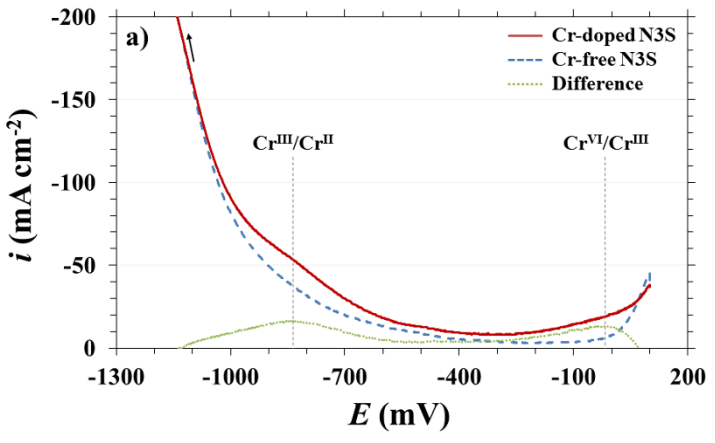

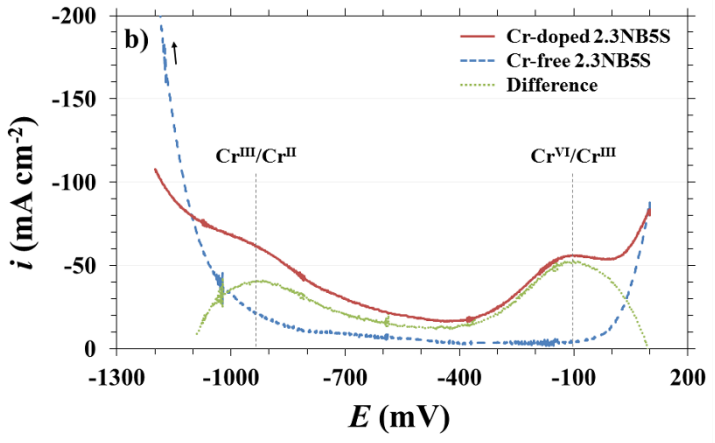

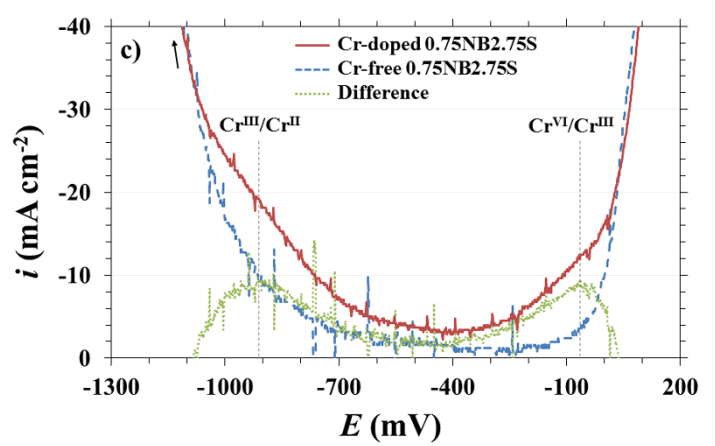

Figure 8: Cr^{III}/Cr^{II} reduction peak current as a function of the square of the square wave frequency f (ΔE_{sw} = 100 mV – 1150°C) in (a) the N3S melt; (b) the 2.3NB5S melt and (c) the 0.75NB2.75S melt.

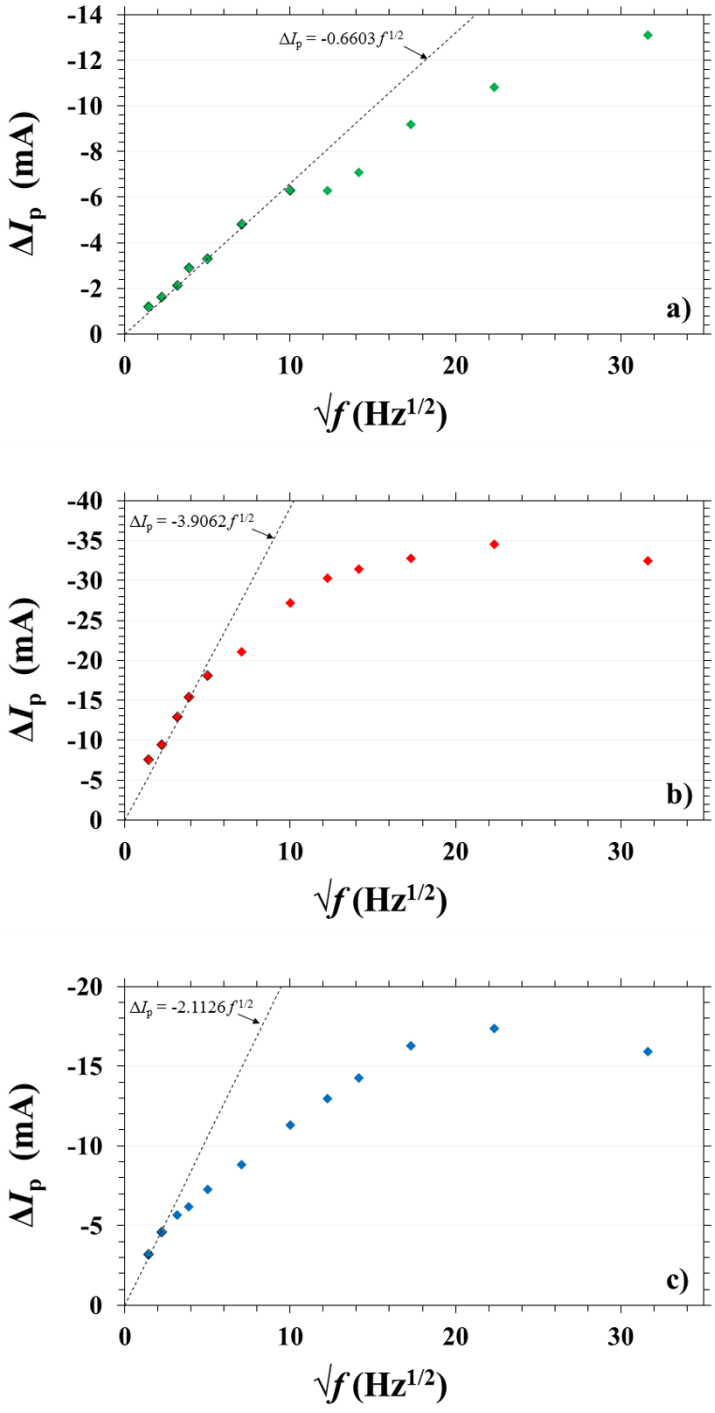

Figure 9: Differential square-wave voltammograms in 2.3NB5S melt showing the evolution of the Cr^{III}/Cr^{II} peak position with scanning frequency.

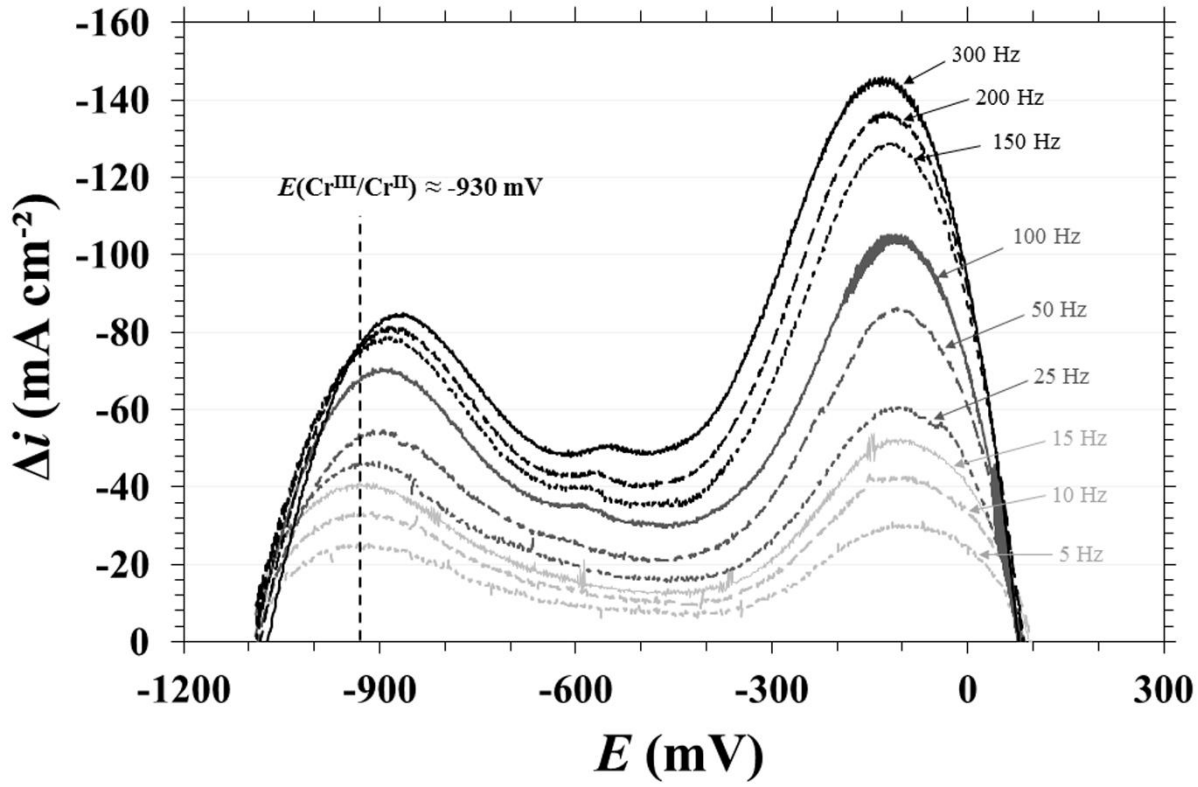

Figure 10: Chromium diffusion coefficients in different glass melt compositions *vs* the melt viscosity at 1150°C, data from this work and literature [13,14,34-36].